AIAA SciTech
4-8 January 2016, San Diego, California, USA
57th AIAA/ASCE/AHS/ASC Structures, Structural Dynamics, and Materials Conference

Reduced Order Gust Response Simulation using Computational Fluid Dynamics

P. Bekemeyer* and S. Timme†

University of Liverpool, Liverpool, England L69 3GH, United Kingdom

The investigation of gust response problems is a crucial and, if high accuracy is desired, time consuming task. Since linear frequency domain methods have previously shown significant reduction in computational cost for motion-induced aerodynamics, an extension towards gust excitation is proposed. Time-domain signals are reconstructed by a superposition of responses at several discrete frequencies. Once frequency domain solutions are available, a reduced order model is constructed projecting the linearised Reynolds-averaged Navier-Stokes equations on a combined modal basis. While eigenmodes are accurate in predicting structural vibration, additional modes from proper orthogonal decomposition capture aerodynamic effects due to gust excitation. For all methods a two-dimensional NACA0012 aerofoil is investigated at sub- and transonic conditions. Limitations of the linearised approach are first outlined by increasing the gust amplitude at both operating points. Subsequently, a worst case gust length search is performed and it is shown that the computational cost is reduced case dependent by several orders of magnitude compared to the original system.

I. Introduction

Gust responses describe critical load cases during the aircraft design process. Highly accurate results at low cost and early stage are desired to investigate a broad range of parameters. Industrial practice is based on linear aerodynamics in frequency domain. While the theories of Theodorsen[1] and Sears[2] are sufficient for simple aerofoil cases, a three-dimensional extension also considering compressibility effects is the doublet lattice method.[3] Examples for this are widespread from isolated wings[4] to full aircraft configurations.[5] Introducing correction factors obtained either from experiments or computational fluid dynamics (CFD) is a well known approach to overcome the lack of accuracy at nonlinear conditions, e.g. high angles of attack or transonic flight speeds.[6] In the past years also CFD aerodynamics alone have been used to investigate gust encounter. While loads are predicted with increased accuracy also at nonlinear conditions, computational cost of time-accurate simulations is overwhelming. However, examples from simple aerofoils to civil aircraft are available.[7–9] Reduced order modelling is considered a reasonable approach to overcome high computational cost when CFD aerodynamics are concerned, while giving accurate results.[10] Several approaches are possible to achieve a reduced order model (ROM) for gust interaction problems including autoregressive methods[8] and eigenvalue realisation.[11]

Another widely spread model reduction technique is based on proper orthogonal decomposition (POD)[12] , which was, with respect to fluid dynamics, first introduced to model coherent structures in turbulent flowfields.[13] A series of snapshots is generated from either experimental or numerical investigations of the full system at several instances in time, while modes are obtained by solving a small eigenvalue problem correlated to these snapshots. The idea of POD using frequency domain sample data was first introduced for the investigation of a rather simple twelve-degrees-of-freedom mass-spring-damper system combined with an incompressible three-dimensional vortex lattice method.[14] An extension towards linearised CFD aerodynamics for a pitch-plunge aerofoil was discussed as well.[15] Snapshots are generated by exciting the system in either pitch or plunge mode at discrete frequencies. An aeroelastic ROM is then formed by projecting

*Ph.D. Student, School of Engineering; philipp.bekemeyer@liverpool.ac.uk.
†Lecturer, School of Engineering; sebastian.timme@liverpool.ac.uk.

the aerodynamic subspace only, while the structural system is retained. An extension to three-dimensional cases, generating snapshots for all structural modes of interest, has also been presented.[16]

The application of system eigenmodes for model reduction is widely spread in combination with linear aerodynamics.[17] These ideas have then been applied to linearised CFD aerodynamics using the Schur complement method to track structural eigenmodes while they are affected by the fluid.[18] Critical eigenmodes can be used in a centre manifold reduction to investigate transonic aeroelastic limit cycle oscillations and perform parameter sensitivity analysis.[19] A model extension for multiple modes is available.[20] While excellent agreement between results from the full nonlinear system and ROM is observed for free response, results are not as satisfying during gust excitation.[21]

In the following, we extend linearised CFD aerodynamics towards gust excitation considering sinusoidal as well as 1-cos gust shapes. Based on this, an aerodynamic ROM is introduced using POD techniques with snapshots generated by exciting sinusoidal gusts at several nonuniformly distributed frequencies. The aerodynamic ROM is then enriched by adding eigenmodes of the coupled fluid-structure Jacobian matrix to discuss aeroelastic problems. A biorthonormal basis is achieved by applying the two-sided Gram-Schmidt algorithm. All techniques are demonstrated using a two-dimensional NACA0012 aerofoil in sub- and transonic regime. Limitations of the linearised approach are outlined by increasing the gust amplitude. The relative information content retained inside the system is discussed as well as the first POD mode. Furthermore, a worst case gust length analysis is performed at both conditions. Finally, computational cost is compared to an equivalent analysis using nonlinear time-marching simulations.

II. Theoretical Formulation

A. Introducing Linearised Aerodynamics

The full order nonlinear system is first presented. The state-space vector $\mathbf{w}$ of size n can be written as

$$\mathbf{w} = \left[\mathbf{w}_\mathrm{f}^T, \mathbf{w}_\mathrm{s}^T\right]^T \tag{1}$$

where $\mathbf{w}_\mathrm{f}$ and $\mathbf{w}_\mathrm{s}$ denote fluid and structural degrees-of-freedom, respectively. While the size of $\mathbf{w}_\mathrm{s}$ is rarely larger than one hundred using a modal structural model, the fluid degrees-of-freedom can be many millions. The governing equation in semi-discrete form is

$$\dot{\mathbf{w}} = \mathbf{R}(\mathbf{w}, \mathbf{v}_\mathrm{g}) \tag{2}$$

where $\mathbf{R}$ is the nonlinear residual corresponding to the unknowns and $\mathbf{v}_\mathrm{g}$ denotes external disturbances due to gusts. The difference between an equilibrium solution $\mathbf{w}_0$ and the state-space vector $\mathbf{w}$ is introduced as

$$\Delta\mathbf{w} = \mathbf{w} - \mathbf{w}_0 \tag{3}$$

and accordingly for external disturbances. The residual in Eq. (2) is expressed around the equilibrium point assuming small motions using a first order Taylor expansion

$$\Delta\dot{\mathbf{w}} = \mathbf{R}(\mathbf{w}_0, \mathbf{v}_{\mathrm{g}0}) + \frac{\partial\mathbf{R}}{\partial\mathbf{w}}\Delta\mathbf{w} + \frac{\partial\mathbf{R}}{\partial\mathbf{v}_\mathrm{g}}\Delta\mathbf{v}_\mathrm{g} \tag{4}$$

where $\mathbf{R}(\mathbf{w}_0, \mathbf{v}_{g0}) = 0$ and $\frac{\partial\mathbf{R}}{\partial\mathbf{w}}$ denotes the Jacobian matrix A.

The system is transferred into linear frequency domain by assuming harmonic motions for the disturbance vector $\Delta\mathbf{w}$ and external excitation vector $\Delta\mathbf{v}_\mathrm{g}$. After rearranging, Eq. (4) becomes

$$\left(A - i\omega I\right)\hat{\mathbf{w}} = -\Xi(\omega)\frac{\partial\mathbf{R}}{\partial\mathbf{v}_\mathrm{g}}\hat{\mathbf{v}}_\mathrm{g} \tag{5}$$

with $\hat{\mathbf{w}}$ and $\hat{\mathbf{v}}_\mathrm{g}$ denoting complex-valued vectors of amplitudes. In Sec. III results are also presented considering the aerodynamic subsystem only. The corresponding equation is

$$\left(A_\mathrm{ff} - i\omega I\right)\hat{\mathbf{w}}_\mathrm{f} = -\Xi(\omega)\frac{\partial\mathbf{R}_\mathrm{f}}{\partial\mathbf{v}_\mathrm{g}}\hat{\mathbf{v}}_\mathrm{g} \tag{6}$$

For an arbitrary time-domain signal, a superposition of results obtained at several discrete frequencies is necessary. The weighting function $\Xi(\omega)$ is introduced to account for varying influence of responses at these

frequencies on the whole solution. Normalised amplitudes from a Fourier analysis of the time-domain signal (e.g. 1-cos gust) are used as weighting factors.

After obtaining frequency domain results, time-domain solutions are calculated from

$$\mathbf{w}(t) = \mathbf{w}_0 + \sum_{j=1}^{J} \Re\left(\hat{\mathbf{w}}_j e^{i\omega_j t}\right) \tag{7}$$

The whole flowfield is reconstructed and can be used to either investigate loads or flow behaviour. Depending on the number of considered frequencies J and the length of the time-domain signal, this becomes a rather cost expensive task. Instead, it is also possible to calculate loads directly in frequency domain avoiding the huge cost of flowfield reconstruction in the time-domain.

The right-hand side is modified so that all residual evaluations, necessary to calculate the gust influence, can be done upfront. This decreases actual simulation time but increases initial cost. By applying the chain rule the right-hand sides in Eqs. (5) and (6) neglecting the weighting factor become

$$\frac{\partial \mathbf{R}}{\partial \mathbf{v}_\mathrm{g}} \hat{\mathbf{v}}_\mathrm{g} = \frac{\partial \mathbf{R}}{\partial \dot{\mathbf{x}}} \frac{\partial \dot{\mathbf{x}}}{\partial \mathbf{v}_\mathrm{g}} \hat{\mathbf{v}}_\mathrm{g} \tag{8}$$

where $\dot{\mathbf{x}}$ denotes artificial mesh velocities applied to model the gust during the CFD calculation using the field velocity approach. Since the relation between gust disturbance $\mathbf{v}_\mathrm{g}$ and artificial mesh velocity $\dot{\mathbf{x}}$ is simply

$$\dot{\mathbf{x}} = -\mathbf{v}_\mathrm{g} \tag{9}$$

Eq. (8) becomes

$$\frac{\partial \mathbf{R}}{\partial \mathbf{v}_\mathrm{g}} \hat{\mathbf{v}}_\mathrm{g} = -\frac{\partial \mathbf{R}}{\partial \dot{\mathbf{x}}} \hat{\mathbf{v}}_\mathrm{g} \tag{10}$$

The matrix $\frac{\partial \mathbf{R}}{\partial \dot{\mathbf{x}}}$ containing changes in residual due to mesh velocities is precomputed using a finite difference scheme and stored explicitly. Computational cost of this task can be reduced further by evaluating the residual only inside the stencil corresponding to the point where the mesh velocity is applied. A second option to solve Eq. (8) is using a finite difference evaluation, applied around the equilibrium point, with a known gust shape vector $\hat{\mathbf{v}}_\mathrm{g}$ to avoid forming and storing the matrix $\frac{\partial \mathbf{R}}{\partial \dot{\mathbf{x}}}$ explicitly. Thus Eq. (10) becomes

$$\frac{\partial \mathbf{R}}{\partial \mathbf{v}_\mathrm{g}} \hat{\mathbf{v}}_\mathrm{g} = \frac{\mathbf{R}(+\varepsilon \mathbf{v}_\mathrm{g}) - \mathbf{R}(-\varepsilon \mathbf{v}_\mathrm{g})}{2\varepsilon} \tag{11}$$

with ε denoting the finite difference step size. Furthermore, an analytical description for the gust vector is introduced as

$$\hat{\mathbf{v}}_\mathrm{g}(\mathbf{x}, \omega) = v_{gz} e^{i\boldsymbol{\varphi}(\mathbf{x},\omega)} \tag{12}$$

where v_{gz} and $\boldsymbol{\varphi}(\mathbf{x}, \omega)$ denote the constant gust amplitude in z-direction and the phase shift at every point, respectively. This phase shift can either be obtained from a Fourier analysis of the time-domain signal or more elegantly using the analytical expression

$$\boldsymbol{\varphi}(\mathbf{x}, \omega) = \frac{\pi}{2} - \left(\mathbf{x} + x_0 + \frac{L_\mathrm{g}}{2}\right) \omega \tag{13}$$

where L_g and x_0 denote the gust length and gust off-set, respectively. When a 1-cos gust is considered, a constant factor of π needs to be subtracted from Eq. (13) for frequencies between $2i/L_\mathrm{g}$ and $(2i+1)/L_\mathrm{g}$, $(i \in \mathbb{N})$ to match Fourier results. Similar expressions can be derived for horizontal gusts by considering the corresponding amplitude and modifying the phase shift accordingly.

B. Basis from Biorthonormal Eigenmodes

Right and left eigenvectors $\boldsymbol{\phi}_i$ and $\boldsymbol{\psi}_i$ of the system Jacobian matrix A are calculated by solving the eigenvalue problems

$$A\boldsymbol{\phi}_i = \lambda_i \boldsymbol{\phi}_i \quad \text{and} \quad A^T \boldsymbol{\psi}_i = \overline{\lambda}_i \boldsymbol{\psi}_i \quad \text{for} \quad i = 1, \ldots, m \tag{14}$$

where the dimension m is far smaller than the initial system size n. Collecting the eigenvectors, the right and left modal matrices are formed as

$$\Phi_{\mathrm{EMD}} = [\boldsymbol{\phi}_1, \ldots, \boldsymbol{\phi}_m] \quad \text{and} \quad \Psi_{\mathrm{EMD}} = [\boldsymbol{\psi}_1, \ldots, \boldsymbol{\psi}_m] \tag{15}$$

where subscript EMD denotes eigenmode decomposition. Furthermore, it is necessary to normalise the eigenvectors to fulfil the biorthonormality condition

$$\Psi_{\mathrm{EMD}}^H \Phi_{\mathrm{EMD}} = I \tag{16}$$

The Schur complement method is used to calculate eigenmodes using CFD aerodynamics, where in accordance with linear aerodynamics only structural normal modes are tracked while they are affected by the fluid. The coupled direct eigenvalue problem can be written as

$$A\boldsymbol{\phi}_i = \begin{bmatrix} A_{\mathrm{ff}} & A_{\mathrm{fs}} \\ A_{\mathrm{sf}} & A_{\mathrm{ss}} \end{bmatrix} \boldsymbol{\phi}_i = \lambda \boldsymbol{\phi}_i \tag{17}$$

where the eigenvector $\boldsymbol{\phi}_i$ is partitioned just as the state-space vector in fluid and structural contributions. Assuming that the eigenvalue λ is not an eigenvalue of matrix block A_{ff}, the small nonlinear eigenvalue problem

$$S(\lambda)\boldsymbol{\phi}_{\mathrm{s}} = \lambda \boldsymbol{\phi}_{\mathrm{s}} \tag{18}$$

is solved instead, where the matrix $S(\lambda)$ is called the Schur complement of A

$$S(\lambda) = A_{\mathrm{ss}} - A_{\mathrm{sf}}(A_{\mathrm{ff}} - \lambda I)^{-1} A_{\mathrm{fs}} \tag{19}$$

Newton's method is applied to solve Eq. (18) using structural frequencies as an initial guess to the eigenvalue.[18] The adjoint eigenvalue problem for $\boldsymbol{\psi}_i$ can be rearranged in Schur complement form just as well.

C. Basis from Proper Orthogonal Decomposition

Linearised CFD aerodynamics following Eq. (6) is used to generate K snapshots at discrete frequencies with sinusoidal excitation. Since full order operations are required, the computational cost is high. Solutions $\hat{\mathbf{w}}_{\mathrm{f}}$ are stored as columns in the snapshot matrix S as

$$S = \left[\hat{\mathbf{w}}_{\mathrm{f}}^1, \hat{\mathbf{w}}_{\mathrm{f}}^2, \ldots, \hat{\mathbf{w}}_{\mathrm{f}}^K\right] \tag{20}$$

The POD basis Φ_{POD} is obtained as a linear combination of snapshots

$$\Phi_{\mathrm{POD}} = S\boldsymbol{\nu}_k \tag{21}$$

where the vector $\boldsymbol{\nu}_k$ is scaled so that vectors in Φ_{POD} are unit length. The eigenvalue problem of dimension K

$$S^H S \boldsymbol{\nu}_k = \lambda_k \boldsymbol{\nu}_k \tag{22}$$

is solved to ensure the best possible approximation in Eq. (21). Eigenvalues λ_k are real and positive since $S^H S$ is positive definite and symmetric. The relative information content a certain mode λ_k contributes to the system, also often referred to as energy, is given by

$$r_k = \lambda_k \left(\sum_{i=0}^{K} \lambda_i \right)^{-1} \tag{23}$$

and can be used to decrease the number of modes further by only considering those with a high relative information content.

D. Combined Model Basis and Model Reduction

An aeroelastic ROM is introduced to investigate the influence of gusts on structural modes by combining the two bases just introduced as

$$\Phi = \left[\Phi_{\mathrm{EMD}}\ ,\ \overline{\Phi}_{\mathrm{EMD}}\ ,\ \Phi_{\mathrm{POD}}\right] \quad \text{and} \quad \Psi = \left[\Psi_{\mathrm{EMD}}\ ,\ \overline{\Psi}_{\mathrm{EMD}}\ ,\ \Psi_{\mathrm{POD}}\right] \tag{24}$$

where $\Psi_{\mathrm{POD}} = \Phi_{\mathrm{POD}}$. Since only the aerodynamic subsystem is considered to identify Φ_{POD}, all POD modes are padded with zero entries in the structural part. Conjugates of the eigenmodes can be added at no additional cost and are necessary to form a sufficient basis. A biorthonormal set is achieved by applying the two-sided Gram-Schmidt algorithm. It should be noted that the biorthonormalisation can break down and thus a more advanced, and expensive, version of the algorithm can be applied to account for this.[22] However, for all cases investigated in this paper, the basic algorithm is sufficiently robust.

Describing the state-space vector $\hat{\mathbf{w}}$ by

$$\hat{\mathbf{w}} = \Phi\hat{\mathbf{z}} \tag{25}$$

and introducing in Eq. (5), gives after projection with the left modal basis

$$\Psi^H \left(A - i\omega I\right)\Phi\hat{\mathbf{z}} = -\Xi(\omega)\Psi^H \frac{\partial \mathbf{R}}{\partial \mathbf{v}_{\mathrm{g}}}\hat{\mathbf{v}}_{\mathrm{g}} \tag{26}$$

The corresponding ROM for aerodynamics is obtained by using POD modes only and expressing the state-space vector $\hat{\mathbf{w}}_{\mathrm{f}}$ as

$$\hat{\mathbf{w}}_{\mathrm{f}} = \Phi_{\mathrm{POD}}\hat{\mathbf{z}}_{\mathrm{f}} \tag{27}$$

Thus, Eq. (6) becomes after projecting

$$\Psi_{\mathrm{POD}}^H \left(A_{\mathrm{ff}} - i\omega I\right)\Phi_{\mathrm{POD}}\hat{\mathbf{z}}_{\mathrm{f}} = -\Xi(\omega)\Psi_{\mathrm{POD}}^H \frac{\partial \mathbf{R}_{\mathrm{f}}}{\partial \mathbf{v}_{\mathrm{g}}}\hat{\mathbf{v}}_{\mathrm{g}} \tag{28}$$

Solving Eqs. (26) or (28) at a range of frequencies, and reconstructing full order solutions afterwards, is an efficient way to investigate gust encounter for coupled and aerodynamic systems, respectively.

III. Results

Results considering a pitch-plunge aerofoil encountering either a sinusoidal or 1-cos gust are presented. First, several responses are shown to outline that the linearised approach is accurate for gust interaction. Limitations are demonstrated by increasing the gust amplitude causing nonlinearities in the corresponding time-marching solution. Secondly, POD is introduced considering aerodynamics only. Several parameters are varied to ensure a sufficient modal basis is created. Afterwards, the ROM is extended by adding eigenmodes from the system Jacobian matrix to discuss coupled fluid-structure cases. Based on this, a worst case gust length analysis is performed to identify critical conditions and a cost analysis is provided as well. For all cases the Reynolds-averaged Navier-Stokes (RANS) equations are solved.

Operations on the nonlinear system for the aerofoil test case are performed using a meshless scheme solving the RANS equations.[23,24] Turbulence is modelled using the Spalart-Allmaras turbulence model.[25] Gusts are introduced by the field velocity approach which adds an artificial mesh velocity to include gust excitations.[26] The artificial mesh velocity is prescribed according to the investigated gust. While this preserves the gust shape during the calculation, since it is unaffected by numerical dissipation, also the influence of structural movements on the gust is neglected. However, due to a lack of affordable alternatives this is still the most common way to model gusts during a CFD calculation. All linearised systems are solved using an improved version of the generalised minimal residual solver.[27]

The considered test case is a NACA0012 aerofoil free to move in pitch and plunge. Structural parameters are given in Tab. 1 and correspond to previous investigations.[20,28] The mesh used for all RANS calculations consists of 31,567 grid points and the distribution around the aerofoil leading edge is shown in Fig. 1a. Freestream Mach numbers of 0.3 and 0.8, covering sub- and transonic aerodynamics, are investigated for zero degrees angle of attack and a Reynolds number of ten million. Surface pressure distributions for both conditions are shown in Fig. 1b with a strong shock for the higher Mach number. This nonlinearity is considered in the following linearised model and the corresponding ROM, since Eq. (4) is formed around the nonlinear steady-state solution.

Parameter	ω_r	r_α	μ	x_α	x_{ea}	$\overline{U}$
Value	0.343	0.539	100.0	-0.2	0.4	2.0

Table 1. Structural parameters of pitch-plunge aerofoil

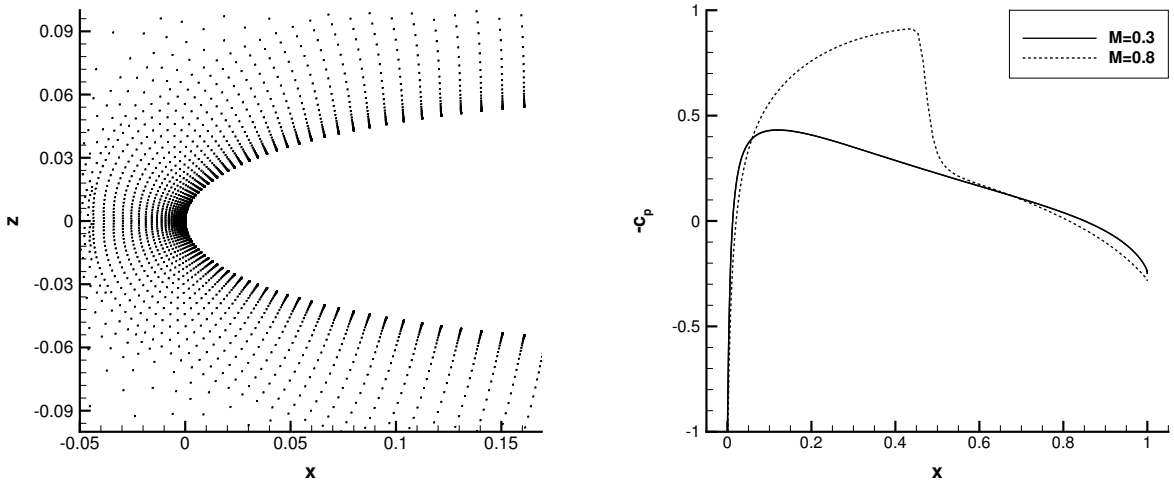

(a) Point distribution around aerofoil

(b) Steady surface pressure distribution

Figure 1. Point distribution and steady-state surface pressure for NACA0012 aerofoil

A. Linear Frequency Domain Aerodynamics for Gust Encounter

For a sinusoidal gust only the frequency $1/L_g$ related to the gust length is required to capture the system behaviour. Furthermore, the weighting function becomes one. Real and imaginary surface pressure distributions obtained from both the Fourier analysis of the time-domain signal and the linear frequency domain (LFD) simulation are shown in Fig. 2a and b with a normalised gust amplitude of $v_{gz} = 0.01$. Since a symmetric case is investigated only the upper surface is displayed. While at subsonic conditions minor differences occur around the stagnation point, for the transonic test case discrepancies arise around the shock location on both sides of the aerofoil. When the gust amplitude is decreased the nonlinear reference solution converges towards the linearised one in both cases. When time-domain results are reconstructed using Eq. (7) and compared to the nonlinear reference solution, a short initial transient period occurs for the time-accurate simulation, and thus small differences can be found in the time history of the lift coefficient during the first two periods as shown in Fig. 3a. In terms of cost the frequency domain solve is between one and two orders of magnitude faster than the corresponding nonlinear time-marching solution slightly depending on the investigated frequency.

The normalised amplitude of lift coefficient over gust amplitude is shown in Fig. 3b. The gust amplitude is normalised using the free-stream velocity. A constant line is obtained from the linear approach while nonlinear solutions start to differ with increasing gust amplitude. These differences are a measure of nonlinearity induced by the unsteady gust excitation. For both Mach numbers results are matching for small amplitudes. This shows that the linearised approach is capable of representing motion around nonlinear steady-state solutions. In subsonic conditions the response starts to decrease before it diverges while at transonic conditions no significant drop is observed since the shock dominates the flow field thus inhibiting a decrease in lift. Once the amplitudes are high enough to cause either significant shock movement or separation the unsteady lift increases extensively for both Mach-numbers. Furthermore, it is no longer possible to achieve converged solutions for gust amplitudes above 25% of the free-stream velocity in transonic flow since the excitation generates massive separation.

For 1-cos gusts several LFD results need to be combined. Applying the analytical phase description and weighting function as outlined in Sec. II, Eq. (6) is solved for multiple frequencies. The number of

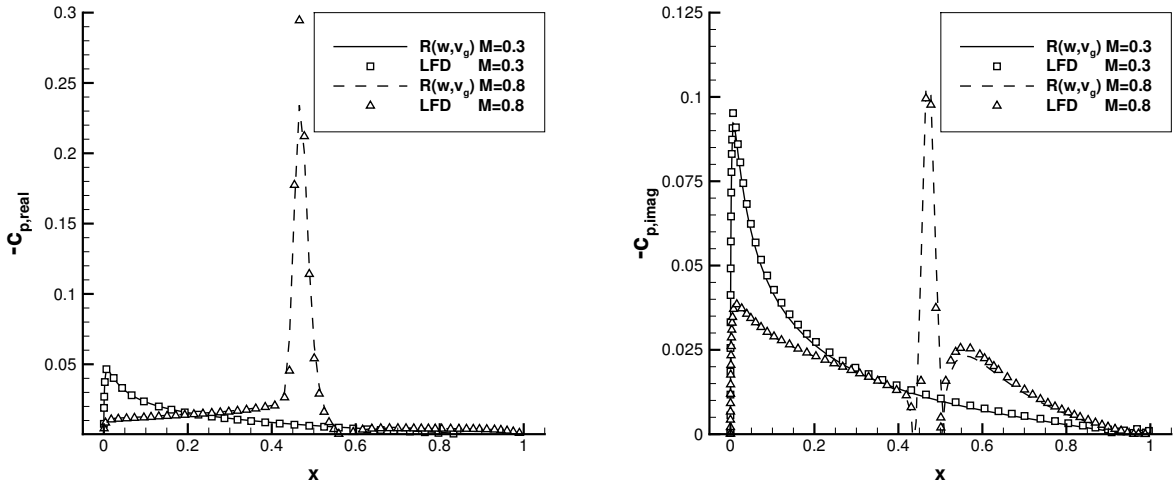

(a) Real part (b) Imaginary part

Figure 2. Complex surface pressure coefficients for a sinusoidal gust with gust length $L_g = 10$

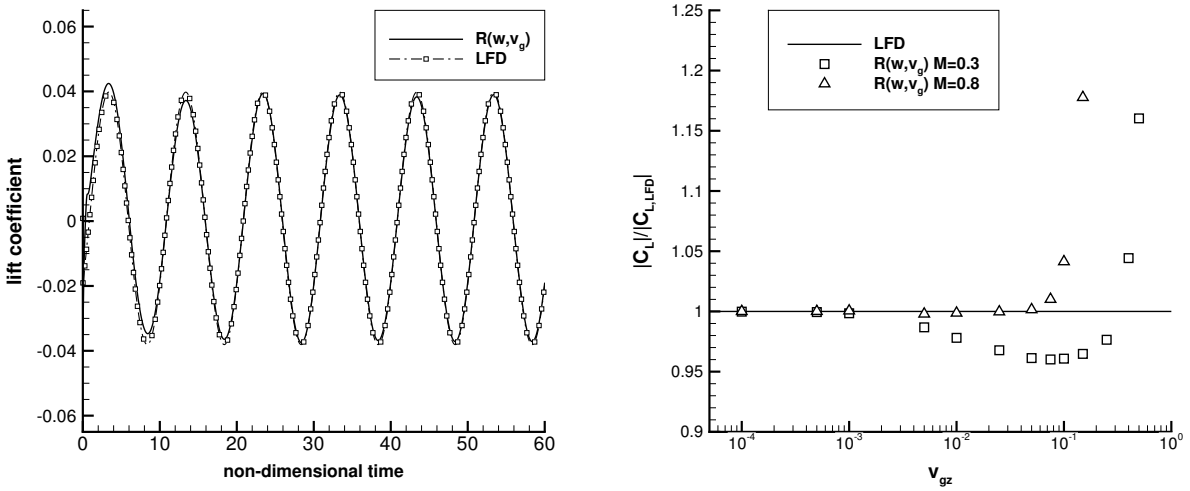

(a) lift coefficient over non-dimensional time M = 0.3 (b) amplitude of lift over gust amplitude

Figure 3. Gust response for a sinusoidal gust with gust length $L_g = 10$

equally spaced frequencies J needs to be adjusted based on the gust length. While for longer gusts only a few frequencies are necessary, for shorter gusts this number is increasing. For instance, 15 frequencies for $L_g = 20$ and 45 frequencies for $L_g = 5$ are required to achieve an error below 1% for the maximum lift coefficient. The main shape of the 1-cos gust is covered by lower frequencies, while higher frequencies are suppressing unwanted oscillations. Including even more frequencies has no influence on integrated loads while still slightly affecting the overall flowfield. Also an exponential distribution function has been tested but no advantages were observed. Afterwards, time-domain results are reconstructed using Eq. (7) adjusting J accordingly. In Fig. 4 results are shown comparing LFD to nonlinear time-domain results for several gust lengths. Good agreement is observed in both sub- and transonic cases with minor discrepancies before the gust interacts with the aerofoil and during the lift decay. Again the shock at transonic conditions stabilises the flowfield and suppresses oscillation that occur during the lift decay for $L_g = 5$ in subsonic conditions.

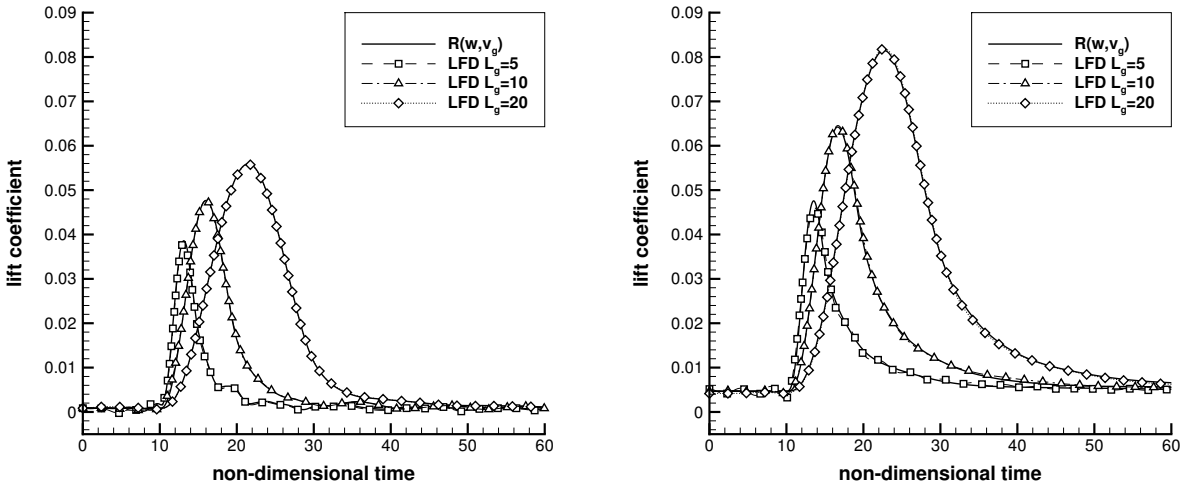

(a) M = 0.3 (b) M = 0.8

Figure 4. Lift coefficient over non-dimensional time for 1-cos gusts with gust lengths of $L_g = 5$, 10 and 20

B. Aerodynamic Reduced Order Model using POD

The aerodynamic ROM based on proper orthogonal decomposition is discussed next. Several parameters are varied to ensure a sufficient modal basis for a broad range of gust encounters. All POD modes are calculated assuming a fixed aerofoil and considering positive frequencies only. However, the complex conjugate of each snapshot can be added at no extra cost which doubles the number of entries in the snapshot matrix and thus possible modes.[15]

Snapshots are calculated using the exponential distribution function

$$f_j = f_0 + \frac{1}{e^{j\Delta f}} \tag{29}$$

to represent the frequency range of interest for various gusts. Other distribution functions such as linear and gradual increase with varying spacings have been tested. In order to achieve results with the same accuracy the exponential distribution offers, more than double the number of snapshots were required. It should be noted that the snapshot sampling is not related to the sampling of frequencies to investigate a discrete time-domain signal. While for snapshots an exponential distribution offers advantages to gather information for different gusts, for a 1-cos gust no clear differences could be observed between different distribution functions.

The ROM is created with 40 snapshots based on Eq. (29) using $f_0 = 0.0$ and $\Delta f = 0.125$ to ensure a broad range of gust lengths can be captured without recalculating the POD basis. As outlined before, the complex conjugate of each snapshot can be added at no additional cost, doubling the number of possible POD modes. The relative information content a certain mode contributes to the system is shown in Fig. 5a after sorting in descending order. For the transonic case over 98% of the information content is covered by the first mode and still 85% at subsonic conditions. From the second mode on, both cases share a gradual decrease until roughly 50 modes, followed by an even steeper decrease until values become numerically zero.

The influence of energy retained inside the ROM is investigated using a 1-cos gust with $L_g = 10$ and $x_0 = 10$. In contrast to linear solves of the full system the spacing and number of considered frequencies for solving Eq. (28) is of minor interest since the system is very small. Time histories for lift coefficient are shown in Fig. 5b. If 99.99% of the relative information content is included the time-domain signal is rebuild accurately. When the amount of information is decreased the peak value increases and oscillations during the lift decay occur while the global shape is preserved. For 98% the overall tendency is still correct but besides the peak value also the lift decrease is no longer represented. For all following results $r_k = 99.99\%$ is retained to identify occurring loads precisely, resulting in 28 modes in subsonic and 18 in transonic since nearly all information is already contained in the first mode. Thus, a huge reduction is achieved compared to the

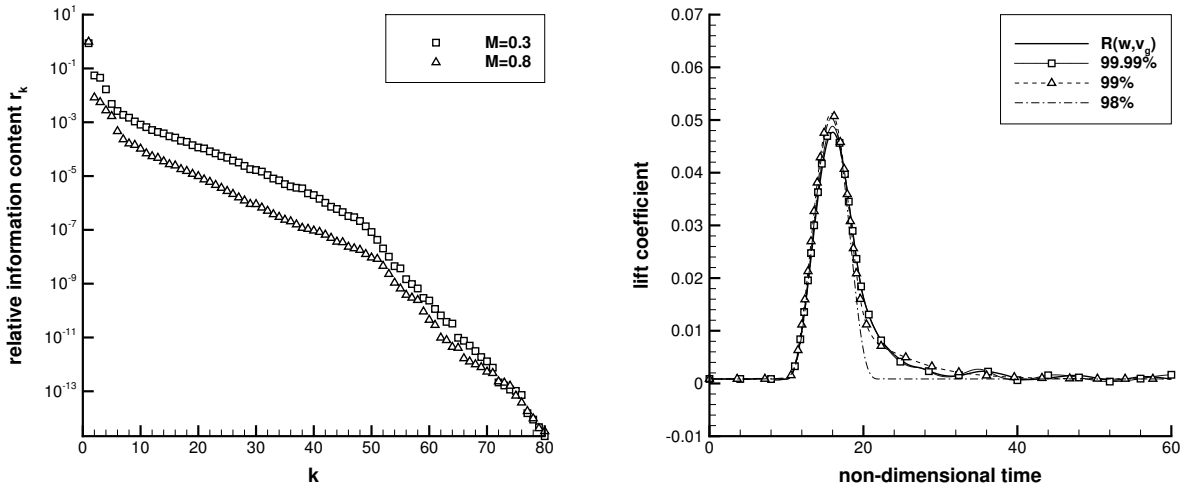

(a) relative information content r_k for 40 snapshots (b) 1-cos gust with varying numbers of POD modes

Figure 5. Investigation of modes retained in POD ROM

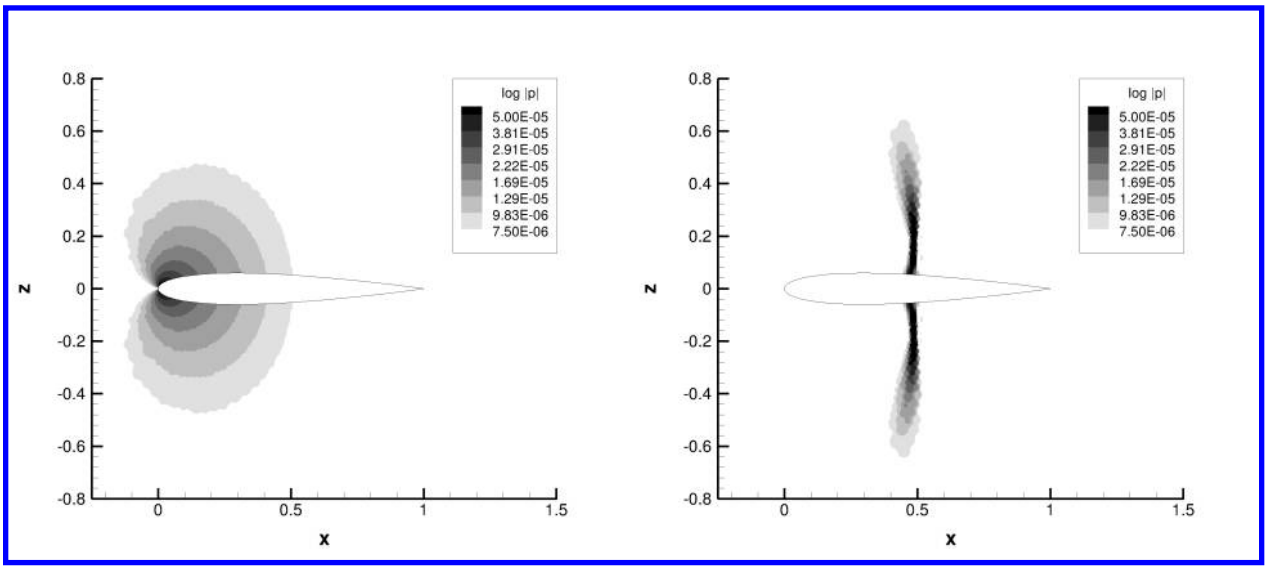

(a) M = 0.3 (b) M = 0.8

Figure 6. Magnitude of pressure for the first POD mode

157,835 degrees-of-freedom of the full system. Subsequently, this basis can be applied to several 1-cos gusts with good agreement for various gust lengths and off-sets. It should be noted, that using a criterion based on r_k rather than retaining a fixed number of modes offers the ROM the capability to adjust to different flow conditions.

The magnitude of pressure for the first POD mode is shown in Fig. 6. Since a symmetric case is investigated the behaviour on upper and lower side of the aerofoil are the same. This mode highlights the area where the flowfield is affected strongest. In transonic conditions the shock region is clearly visible, while in subsonic conditions the suction around the leading edge can be seen. Small values in both plots are caused by the scaling of POD modes, necessary to achieve orthonormality. The slightly uneven flowfield results from the post-processing interpolation of the point centred data.

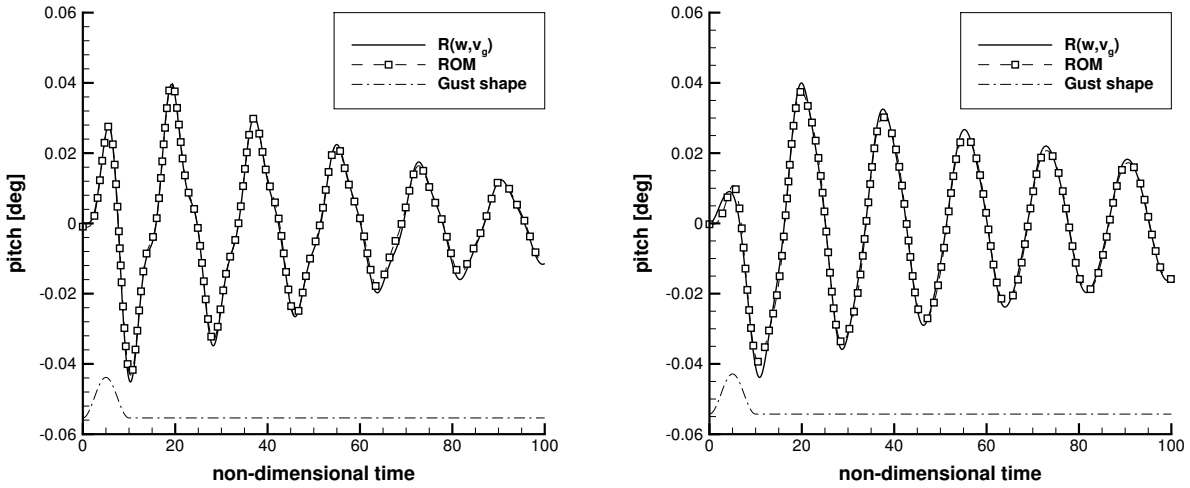

(a) M = 0.3 (b) M = 0.8

Figure 7. Pitch over time for 1-cos gust with $L_g = 10$ obtained from ROM and nonlinear reference solution

Task	Cost(sec)
Time-domain simulation	36,000
Reduced order model build-up (total cost)	8100
a) Calculating EMD basis	1200
b) Calculating snapshots and POD basis	6800
c) Calculating gust influence matrix	10
d) Combining bases and biorthonormalisation	90
Coupled ROM LFD for 1-cos gust	10
Post-processing	
a) Rebuilding whole solution	186
b) Rebuilding only structural d.o.f.	1

Table 2. Comparison of computational cost

C. Aeroelastic Reduced Order Model using a Combined Basis

The ROM presented in the following section consists of POD modes to cover gust influences and eigenmodes to account for structural motion. The modal basis is obtained as outlined before, where number and spacing of snapshots are chosen based on the results presented in Sec. III B. The resulting subsonic model consists of 32 modes where four modes are related to eigenmodes and their corresponding complex conjugate and 28 to POD. In transonic conditions the total number of modes is 22 of which 18 are POD modes.

Since the frequency spacing and number of considered frequencies is of minor influence on the computational cost, it should, however, be ensured that low frequencies are included as well as several frequencies around the structural eigenfrequencies to resolve gust excitation and structural motion accurately. Reconstructed time-domain signals for pitch are shown in Fig. 7 together with nonlinear reference solutions. The displayed gust shape is related to the leading edge. For both Mach numbers good agreement is observed besides minor differences for the peak values due to nonlinearities. Similar results are obtained for different gust lengths and off-sets.

A comparison of computational cost necessary to obtain nonlinear reference solutions and ROM results including cost to generate the model are shown in Tab. 2. For nonlinear simulations a non-dimensional time step size of 0.02 and 5000 time steps were used. While the build-up cost of the ROM is high, it occurs only

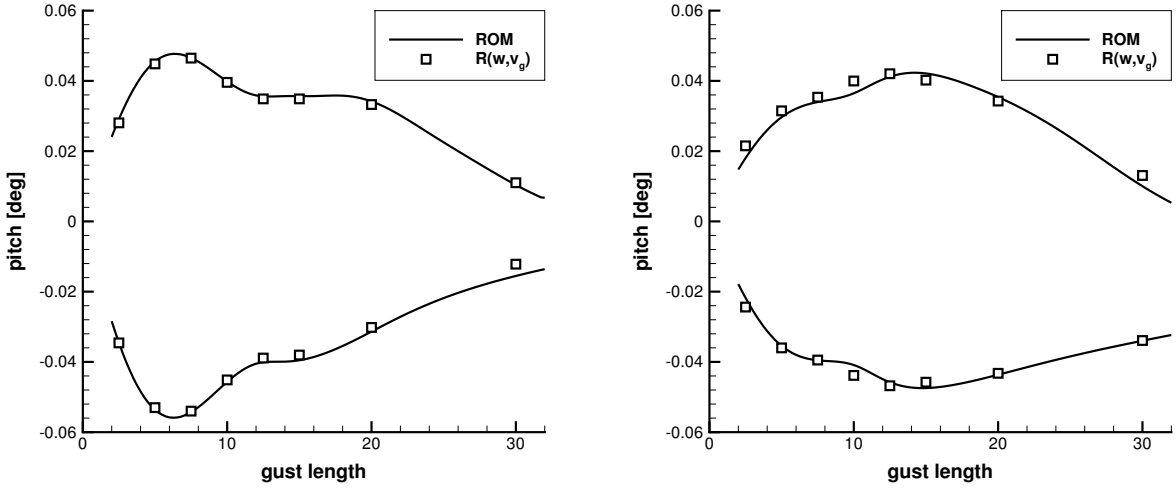

(a) M = 0.3 (b) M = 0.8

Figure 8. Worst case gust length for pitch

once for a given set of flight parameters (e.g. Mach number or angle of attack) and is independent from the investigated gust shape including gust length and off-set. The time-domain simulation on the other hand needs to be redone for any parameter change. Since decreasing gust lengths increase the required frequency range, the time necessary for shorter gust lengths is increased. Therefore, time shown for an LFD analysis of the ROM is an average value obtained for several gust lengths. Furthermore, the reduced model needs post-processing where the frequency response is transferred into time-domain which can be a cost expensive task. This cost can be significantly decreased by reconstructing only time-domain histories for structural degrees-of-freedom. Overall, a ROM solve is faster by three orders of magnitude.

The ROM is now applied for gust lengths between $L_g = 2$ and 32 using an increment of $\Delta L_g = 0.1$ and a constant gust amplitude of $v_{gz} = 0.01$ at both Mach numbers to identify the worst case gust length. Results for pitch are shown in Fig. 8 together with several reference solutions. For both Mach numbers the ROM correctly predicts the system behaviour. In subsonic flow the worst case gust length is predicted at $L_g \approx 6.0$ which correlates to the angular frequency of the pitch mode affected by the fluid at $\omega_\alpha = 1.06$. The plunge mode instead corresponds to a gust length of $L_g \approx 17.9$. In transonic, the worst case gust length is shifted to $L_g \approx 14.4$. In addition, results starts to differ from the reference solution since nonlinearities are arising which are not covered by the reduced model. The time necessary to perform the worst gust length search is roughly 30 minutes using the ROM while the full order equivalent would have taken several days.

IV. Conclusions

This paper outlines a method to compute the aerodynamic and structural response to gust encounter. The governing equations are linearised to obtain responses to sinusoidal gusts, a method previously only used for motion-induced aerodynamics. Arbitrary time-domain signals such as 1-cos gusts can be simulated using a weighted superposition of responses at discrete frequencies. Computational cost is reduced further by introducing proper orthogonal decomposition. Snapshots are calculated based on the former outlined linearised approach at nonuniformly distributed frequencies. Fluid-structure cases are analysed by enriching the modal basis with eigenmodes of the coupled Jacobian matrix.

The test case presented is a simple NACA0012 aerofoil in sub- and transonic conditions. Complex surface pressure distributions are shown with good agreement for both flight conditions. For the POD model, snapshots are calculated based on the linearised approach at exponentially distributed frequencies. The relative information content retained inside the system is investigated and the first POD mode is discussed. After enriching the reduced modal basis by eigenmodes of the coupled Jacobian matrix, structural responses are shown and a worst case gust length search is performed with satisfying results. In terms of computational

cost the ROM offers an improvement of three orders of magnitude for a single response and several orders of magnitude for a worst case gust length search.

An extension towards a three-dimensional industrial relevant test case for both the linearised approach and the reduced order model is currently in progress. Also, it is desirable to conciser nonlinear effects to increase the accuracy of predicted loads further in transonic conditions where nearly all aircraft operate nowadays. Furthermore, transferring the ROM into time-domain is currently investigated to simplify the inclusion of a control system and speed up post-processing by avoiding the inverse Fourier transform.

Acknowledgements

The research leading to these results was co-funded by Innovate UK, the UK's innovation agency, as part of the Enhanced Fidelity Transonic Wing project.

References

[1]Theodorsen, T., "General Theory of Aerodynamic Instability and the Mechanism of Flutter," *NACA Report*, , No. 496, 1935, pp. 413–433.

[2]Sears, W. R., "On the Reaction of an Elastic Wing to Vertical Gusts," *Journal of the Aeronautical Sciences*, Vol. 8, No. 2, 1941, pp. 64–67.

[3]Albano, E. and Rodden, W. P., "A doublet lattice method for calculating lift distribution on oscillating surfaces in subsonic flow," *AIAA Journal*, Vol. 2, No. 7, 1969, pp. 279–285.

[4]Giesing, J. P., Rodden, W. P., and Stahl, B., "Sears Function and Lifting Surface Theory for Harmonic Gust Fields," *Journal of Aircraft*, Vol. 7, 1970, pp. 252–255.

[5]Kier, T., "Comparison of Unsteady Aerodynamic Modelling Methodologies with Respect to Flight Loads Analysis," *AIAA Atmospheric Flight Mechanics Conference and Exhibit*, 2005, AIAA Paper 2005-6027.

[6]Dimitrov, D. and Thormann, R., "DLM-Correction Methods for Aerodynamic Gust Response Prediction," *International Forum on Aeroelasticity and Structural Dynamics (IFASD)*, 2013, IFASD 2013-24C.

[7]Wales, C., Jones, D., and Gaitonde, A., "Prescribed Velocity Method for Simulation of Aerofoil Gust Responses," *Journal of Aircraft*, 2015, pp. 64–76.

[8]Raveh, D. E., "CFD-Based Models of Aerodynamic Gust Response," *Journal of Aircraft*, Vol. 44, No. 3, 2007, pp. 888–897.

[9]Reimer, L., Ritter, M., Heinrich, R., and Krüger, W., "CFD-based Gust Load Analysis for a Free-flying Flexible Passenger Aircraft in Comparison to a DLM-based Approach," *22nd AIAA Computational Fluid Dynamics Conference*, 2015, AIAA 2015-2455.

[10]Lucia, D. J., Beran, P. S., and Silva, W. A., "Reduced-order modeling: new approaches for computational physics," *Progress in Aerospace Sciences*, Vol. 40, No. 1-2, 2004, pp. 51–117.

[11]Wales, C., Gaitonde, A., and Jones, D., "Reduced order modelling for aeroelastic aerofoil response to a gust," *51st AIAA Aerospace Sciences Meeting including the New Horizons Forum and Aerospace Exposition*, 2013, AIAA Paper 2013-0790.

[12]Dowell, E. H. and Hall, K. C., "Reduced Order Models in Unsteady Aerodynamic Models, Aeroelasticity and Molecular Dynamics," *ICAS - 26th Congress of International Council of the Aeronautical Sciences*, 2008, ICAS 2008-0.1.

[13]Lumley, J. L., *The Structures of Inhomogeneous Turbulent Flow*, Atmospheric Turbulence and Radio Wave Propagation, 1965.

[14]Kim, T., "Frequency-Domain Karhunen-Loève Method and Its Application to Linear Dynamic Systems," *AIAA Journal*, Vol. 36, No. 11, 1998, pp. 2117–2123.

[15]Hall, K. C., Thomas, J. P., and Dowell, E. H., "Proper Orthogonal Decomposition Technique for Transonic Unsteady Aerodynamic Flows," *AIAA Journal*, Vol. 38, No. 10, 2000, pp. 1853–1862.

[16]Thomas, J. P., Dowell, E. H., and Hall, K. C., "Three-Dimensional Transonic Aeroelasticity Using Proper Orthogonal Decomposition-Base Reduced-Order Models," *Journal of Aircraft*, Vol. 40, No. 3, 2003, pp. 544–551.

[17]Bisplinghoff, R. L., Ashley, H., and Halfman, R. L., *Aeroelasticity*, 1955.

[18]Badcock, K. J. and Woodgate, M. A., "Bifurcation Prediction of Large-Order Aeroelastic Models," *AIAA Journal*, Vol. 48, No. 6, 2010, pp. 1037–1046.

[19]Woodgate, M. A. and Badcock, K. J., "Fast prediction of transonic aeroelastic stability and limit cycles," *AIAA Journal*, Vol. 45, No. 6, 2007, pp. 1370–1381.

[20]Da Ronch, A., Tantaroudas, N. D., Timme, S., and Badcock, K. J., "Model reduction for linear and nonlinear gust loads analysis," *4th AIAA/ASME/ASCE/AHS/ASC Structures, Structural Dynamics, and Materials Conference*, 2013, AIAA Paper 2013-1492.

[21]Timme, S., Badcock, K. J., and Da Ronch, A., "Linear Reduced Order Modelling for Gust Response Analysis using the DLR-TAU Code," *International Forum on Aeroelasticity and Structural Dynamics (IFASD)*, 2013, IFASD 2013-36A.

[22]Parlett, B. N., "Reduction to Tridiagonal Form and Minimal Realizations," *SIAM Journal on Matrix Analysis and Applications*, Vol. 13, No. 2, 1992, pp. 567–593.

[23]Kennett, D. J., Timme, S., Angulo, J., and Badcock, K. J., "An Implicit Meshless Method for Application in Computational Fluid Dynamics," *International Journal for Numerical Methods in Fluids*, Vol. 71, No. 8, 2013, pp. 1007–1028.

[24]Kennett, D. J., Timme, S., Angulo, J., and Badcock, K. J., "Semi-Meshless Stencil Selection for Anisotropic Point Distributions," *International Journal of Computational Fluid Dynamics*, Vol. 26, No. 9-10, 2012, pp. 463–487.

[25]Spalart, P. R. and Allmaras, S. R., "A One-Equation Turbulence Model for Aerodynamic Flows," *Recherche Aerospatiale*, , No. 1, 1994, pp. 5–21.

[26]Parameswaran, V. and Baeder, J. D., "Indicial aerodynamics in compressible flow-direct computational fluid dynamic calculations," *Journal of Aircraft*, Vol. 34, No. 1, 1997, pp. 131–133.

[27]Xu, S., Timme, S., and Badcock, K. J., "Krylov Subspace Recycling for Linearised Aerodynamics Analysis using DLR-TAU," *International Forum on Aeroelasticity and Structural Dynamics (IFASD)*, 2015, IFASD-2015-186.

[28]Badcock, K. J., Woodgate, M. A., and Richards, B. E., "Hopf Bifurcation Calculations for a Symmetric Airfoil in Transonic Flow," *AIAA Journal*, Vol. 42, No. 5, 2004, pp. 883–892.